Supplementary Materials for "Identifying Snow-Covered Areas from Unoccupied Aerial Systems (UAS) Visible Imagery: A Comparison of Methods"

Mahsa Moradi[1,2], Andrew G. Fleming[1,2], Adam Hunsaker[1,2], Jennifer M. Jacobs[1,2]

[1]Department of Civil and Environmental Engineering, University of New Hampshire, Durham, NH, USA

[2]Earth Systems Research Center, Institute for the Study of Earth, Oceans, and Space, University of New Hampshire, Durham, NH, USA

S1. Estimating Sky Coverage:

The clearness index (K_c) was computed as the ratio between observed shortwave radiation and the estimated clear-sky value:

$$K_c = \frac{SW_{obs}}{SW_{clear}} \quad \text{(S1)}$$

Table S1. Estimated sky condition based on clearness index

Clearness index	Sky Condition
$0.85 < K_c$	Clear
$0.60 < K_c \leq 0.85$	Mostly Clear
$0.35 < K \leq 0.60$:	Partly Cloudy
$K_c \leq 0.35$	Cloudy

To estimate the theoretical clear-sky incoming shortwave radiation (SW_{clear}) at the surface, we used a simplified atmospheric transmissivity model that accounts for solar geometry, time of year, and geographic location. The clear-sky incoming shortwave radiation (W/m²) at a given time and location was estimated as:

$$SW_{clear} = S_0 \times \cos(\theta) \times \tau \quad \text{(S2)}$$

where S_0 is the top-of-atmosphere solar irradiance (W/m²), $\cos(\theta)$ is the cosine of the solar zenith angle, and τ is an empirical atmospheric transmissivity factor (set to 0.7). The extraterrestrial solar irradiance at the top of the atmosphere is calculated as:

$$S_0 = 1367 \times (1 + 0.033 \times \cos(2\pi \frac{\mathrm{DOY}}{365}) \quad \text{(S3)}$$

where DOY is the day of the year and 1367 W/m² is the solar constant. The cosine of the solar zenith angle is computed using:

$$\cos(\theta) = (\sin(\phi) \times \sin(\delta)) + (\cos(\phi) \times \cos(\delta) \times \cos(h)) \quad \text{(S4)}$$

where: ϕ is the latitude in radians, δ is the solar declination angle in radians, and h is the solar hour angle in radians. The solar declination angle is given by:

$$\delta = 23.45\sin\left(\frac{360(284+\mathrm{DOY})}{365}\right) \quad \text{(S5)}$$

The hour angle h depends on the local solar time (in decimal hours) and is calculated as:

$$h = 15(Solar\ Time - 12) \quad \text{(S6)}$$

To correct for solar time, we accounted for both longitude and the Equation of Time (EoT, the difference between apparent solar time and mean solar time):

$$Solar\ Time = \mathrm{Clock\ Time} + \left(\frac{(4(\lambda\mathrm{std} - \lambda) + E_o\mathrm{T})}{60}\right) \quad \text{(S7)}$$

$$E_oT = 9.87\sin(2\mathrm{B}) - 7.53\cos(\mathrm{B}) - 1.5\sin(\mathrm{B}) \quad \text{(S8)}$$

$$B = 360\frac{DOY-81}{365} \quad \text{(S9)}$$

where:

λ_{std} is the standard meridian for the time zone (in degrees), λ is the local longitude (in degrees), and Clock Time is the local time of day in decimal hours.

Table S2. Mean balanced accuracies for different static blue band thresholds, averaged over five trials each. The optimal threshold (135) is bolded.

Threshold	Mean Balanced Accuracy
95	0.732
105	0.769
115	0.797
127	0.828
135	**0.849**
145	0.825

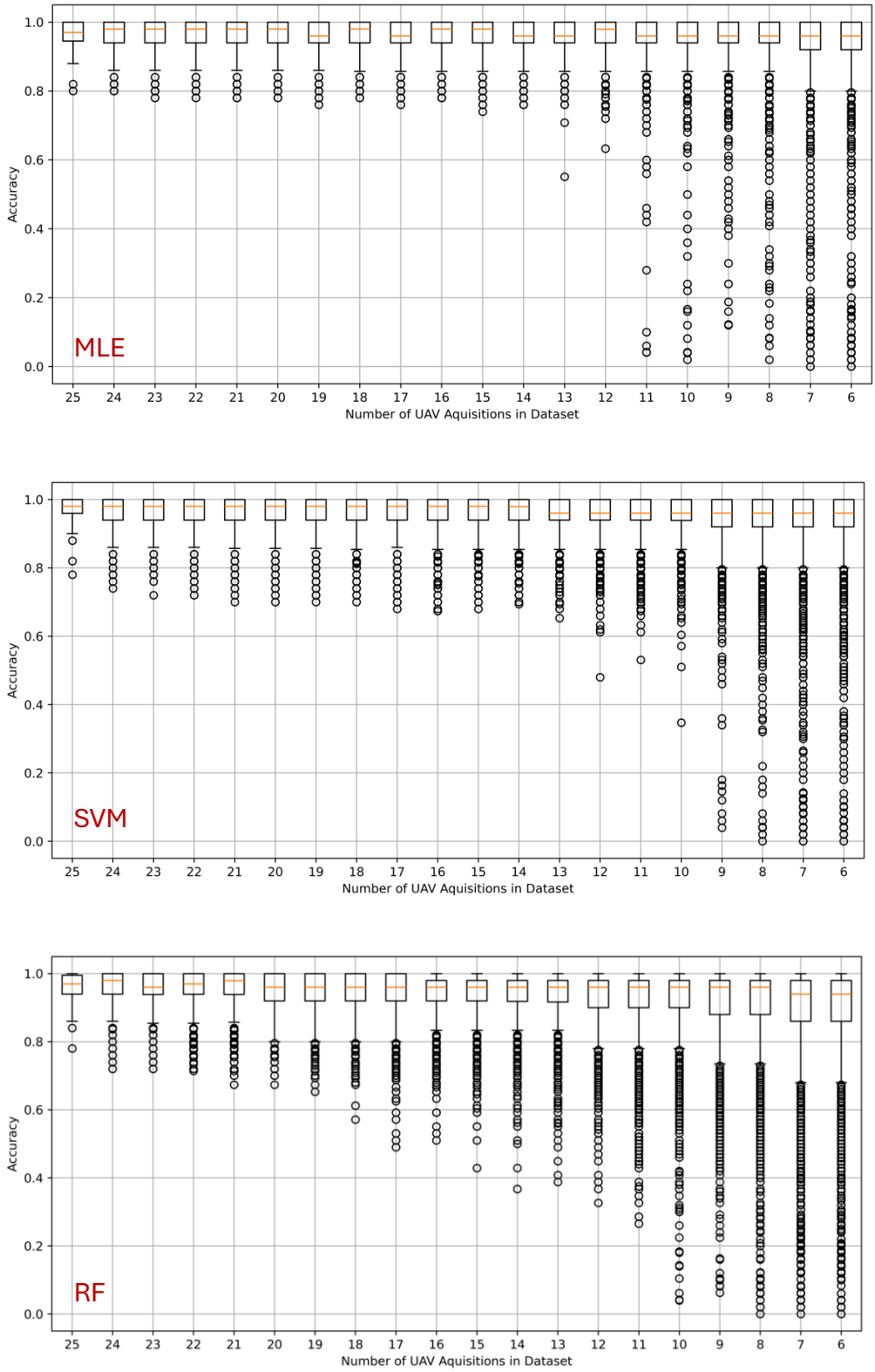

Figure S-1. Accuracy of the three classifiers on left-out orthomosaics, shown in relation to the number of orthomosaics included in the dataset. Top is MLE, middle is SVM, and bottom is RF.

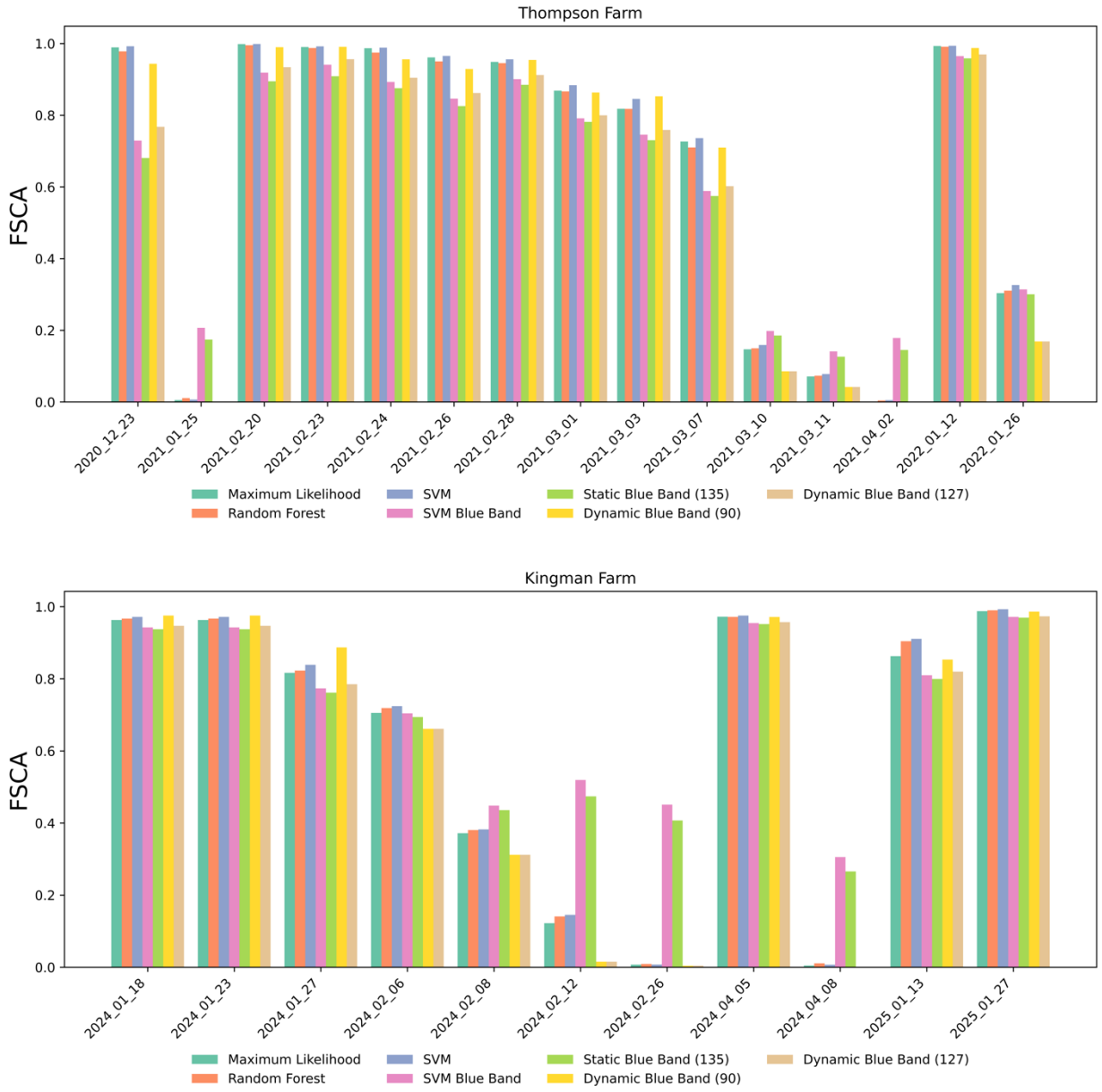

Figure S-2. Comparison of factional snow-covered area (fSCA) across different SCA classification methods for each UAV acquisition date at two study sites (KF and TF). The fSCA is calculated as the proportion of pixels classified as snow relative to the total valid pixels in the orthomosaic.

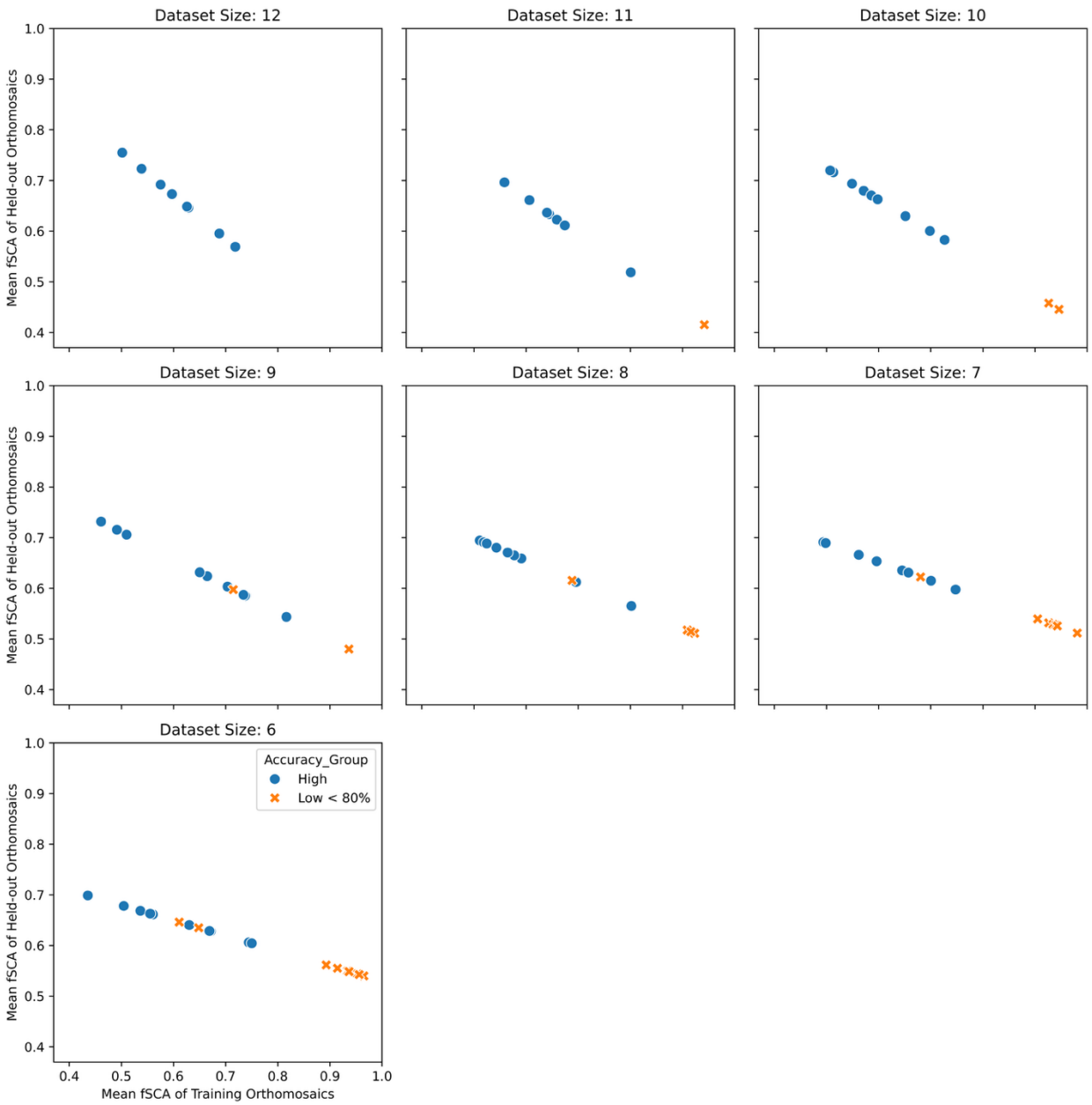

55 **Figure S-3.** Mean fSCA of orthomosaics within training vs. Mean fSCA of held-out orthomosaics for the 20 combinations (10 highest and 10 lowest (<80%) accuracy) for the MLE classifier. Blue dots represent high-accuracy combinations; orange dots represent low-accuracy combinations. The individual plots differ by the number of orthomosaics in the training dataset. Training dataset sizes of 10, 11, and 12 did not have any held-out datasets with accuracy values < 80%.

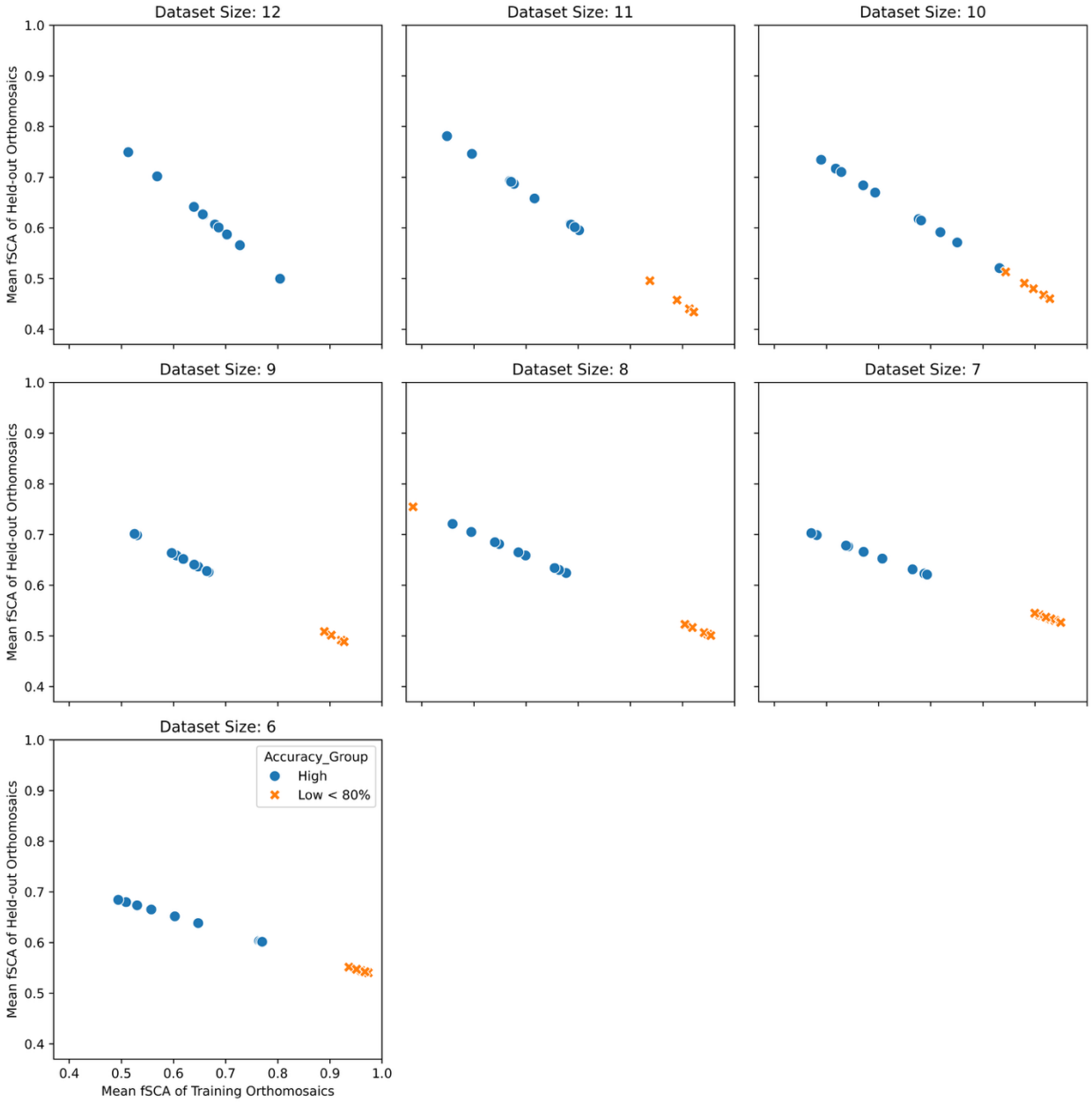

Figure S-4. Mean fSCA of orthomosaics within training vs. Mean fSCA of held-out orthomosaics for the 20 combinations (10 highest and 10 lowest (<80%) accuracy) for the RF classifier. Blue dots represent high-accuracy combinations; orange dots represent low-accuracy combinations. The individual plots differ by the number of orthomosaics in the training dataset. Training dataset sizes of 10, 11, and 12 did not have any held-out datasets with accuracy values < 80%.

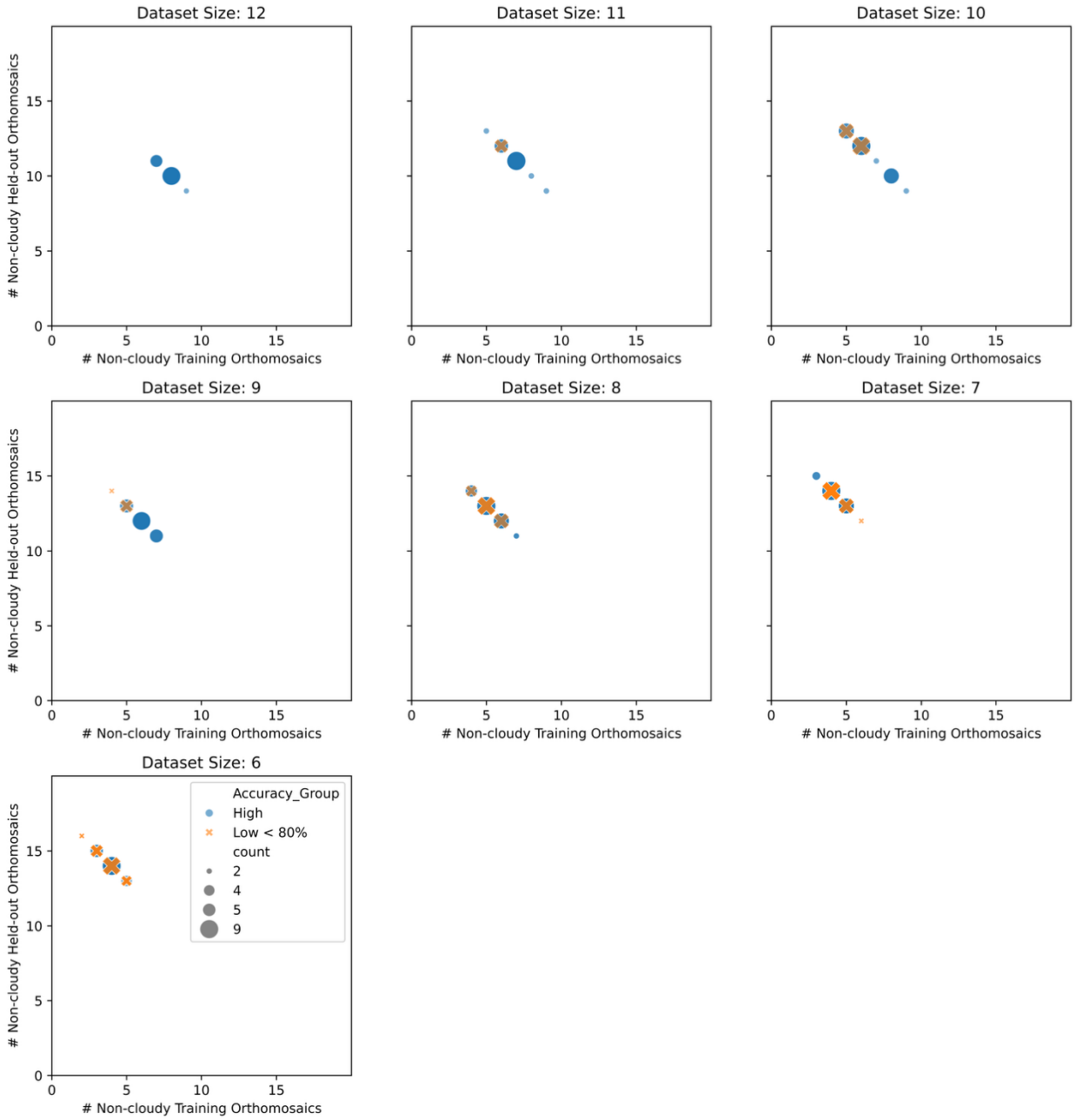

Figure S-5. Number of non-cloudy orthomosaics within training set VS. Number of non-cloudy orthomosaics within held-out set for the 20 combinations (10 highest and 10 lowest (<80%) accuracy) for the MLE classifier. Blue dots represent high-accuracy combinations; orange dots represent low-accuracy combinations

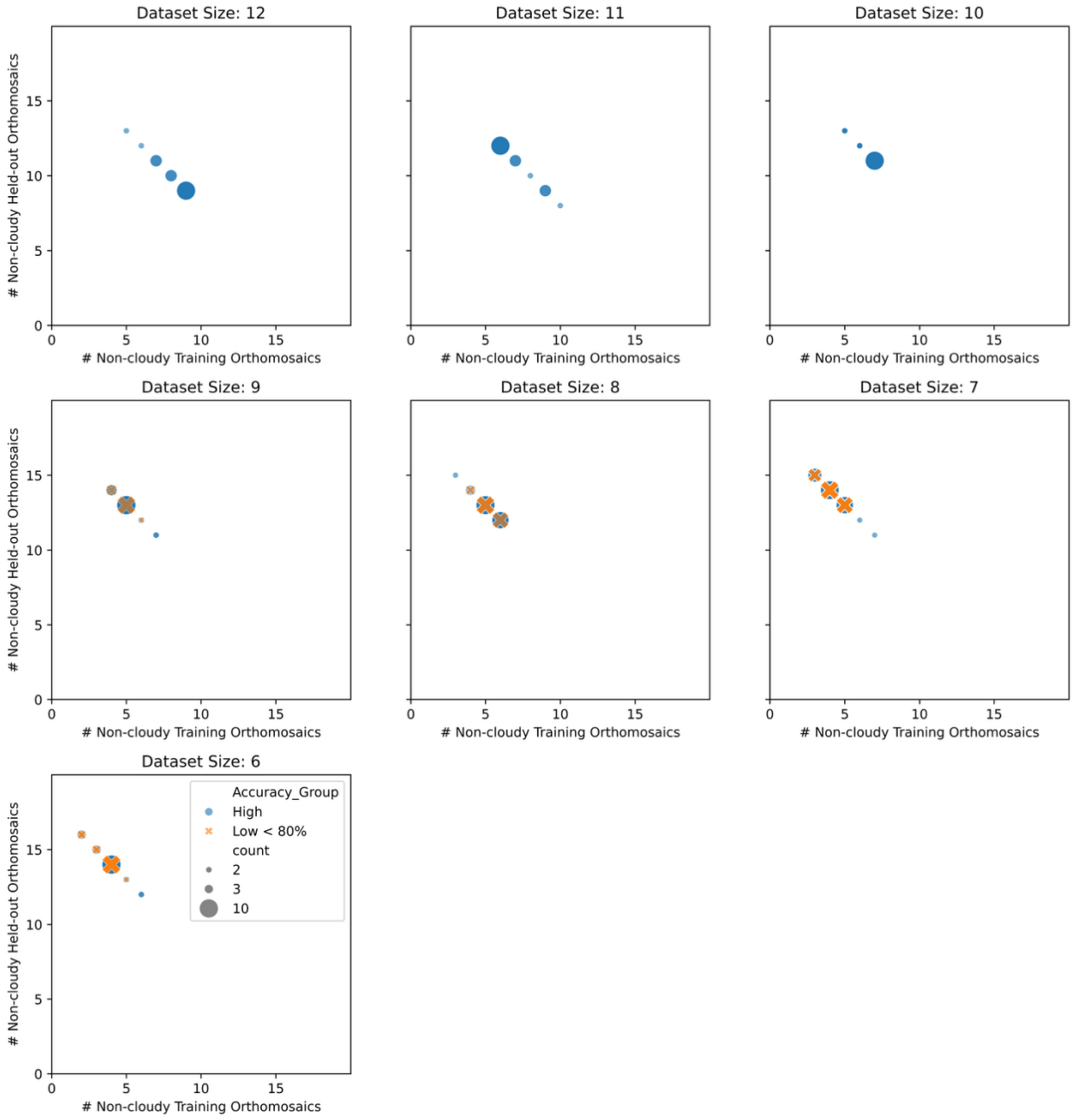

Figure S-6. Number of non-cloudy orthomosaics within training set VS. Number of non-cloudy orthomosaics within held-out set for the 20 combinations (10 highest and 10 lowest (<80%) accuracy) for the SVM classifier. Blue dots represent high-accuracy combinations; orange dots represent low-accuracy combinations

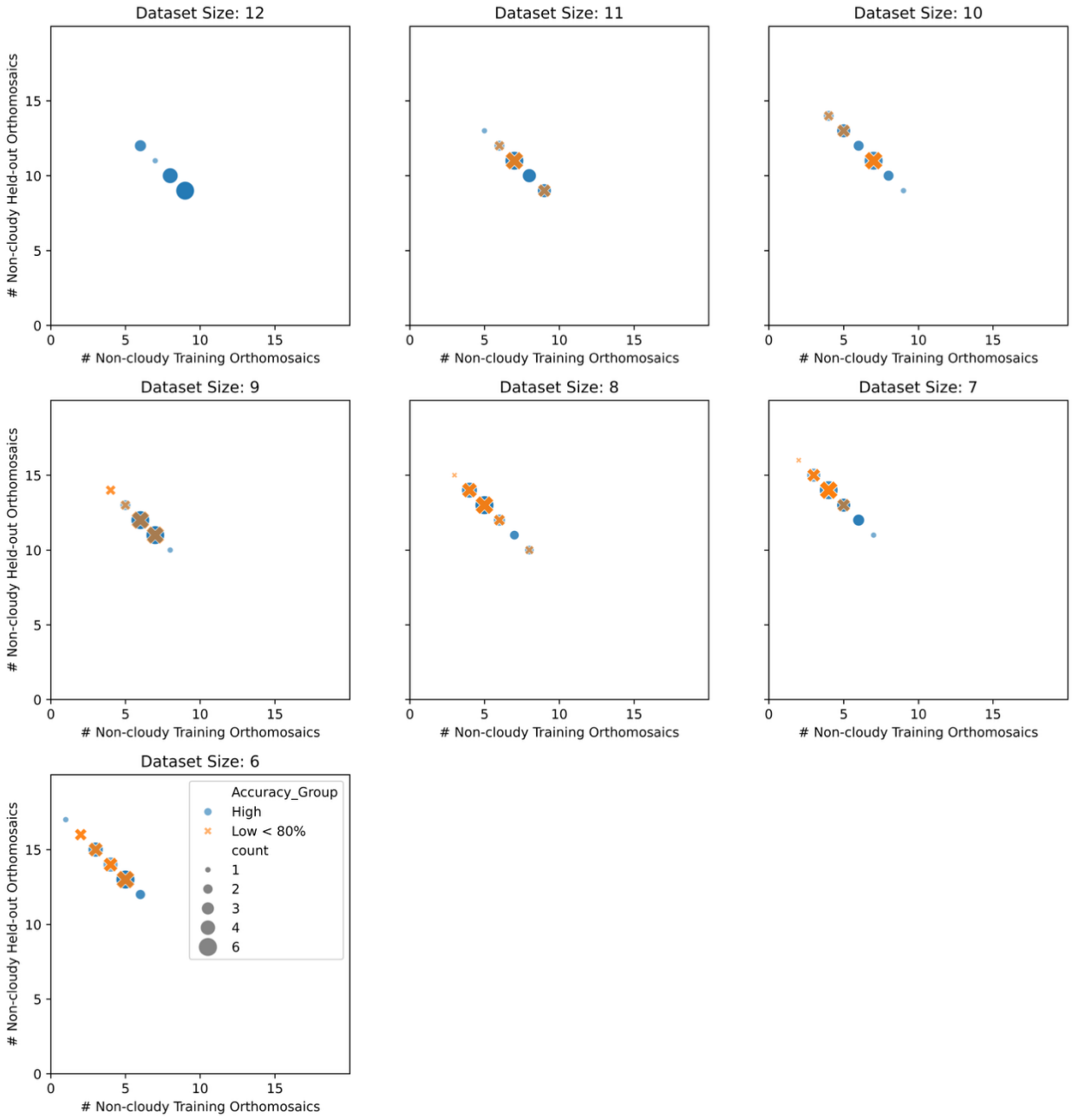

Figure S-7. Number of non-cloudy orthomosaics within training set VS. Number of non-cloudy orthomosaics within held-out set for the 20 combinations (10 highest and 10 lowest (<80%) accuracy) for the RF classifier. Blue dots represent high-accuracy combinations; orange dots represent low-accuracy combinations

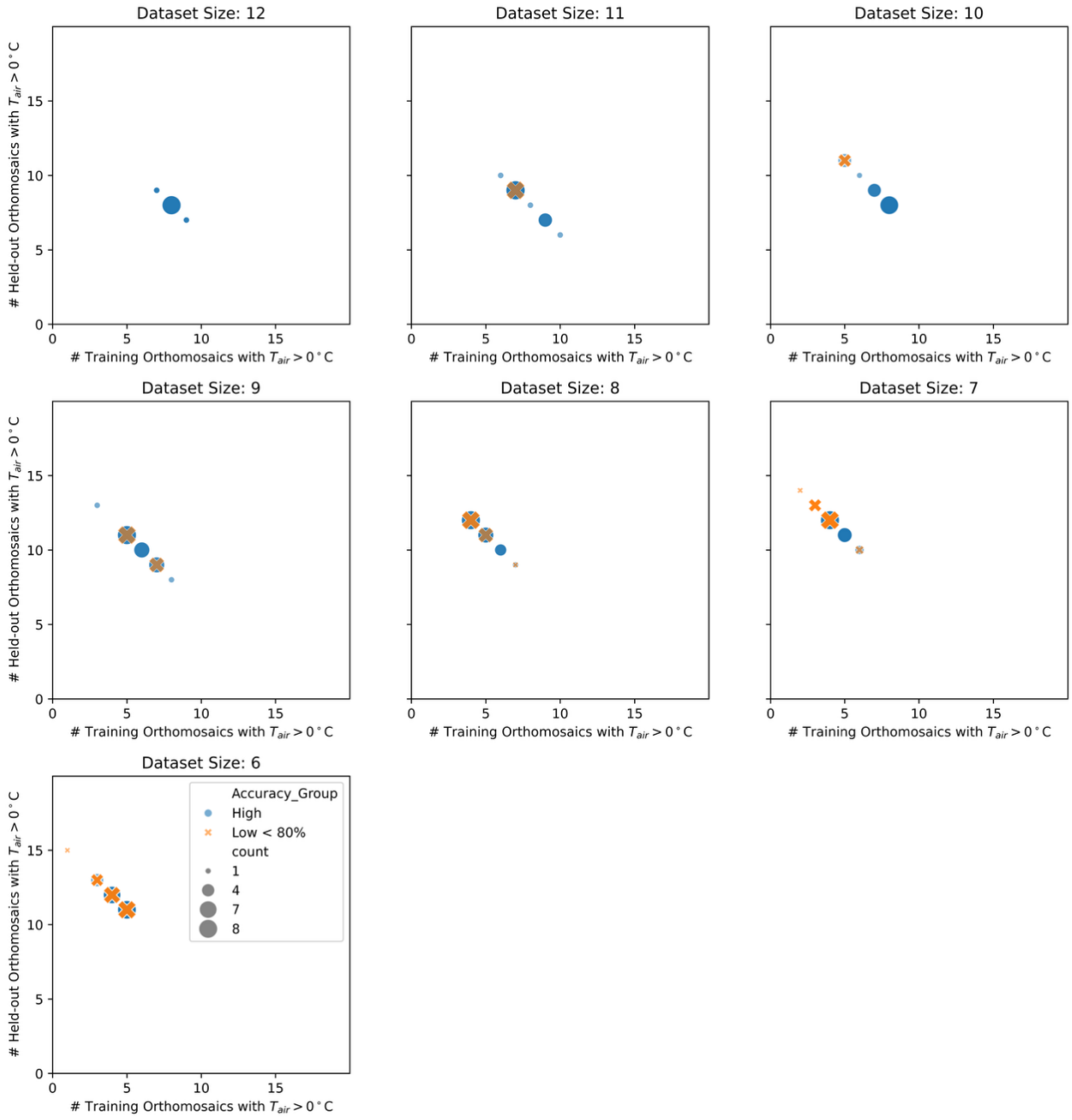

Figure S-8. Number of days with air temperature above freezing within training set VS. Number of days with air temperature above freezing within held-out set for the 20 combinations (10 highest and 10 lowest (<80%) accuracy) for the MLE classifier. Blue dots represent high-accuracy combinations; orange dots represent low-accuracy combinations

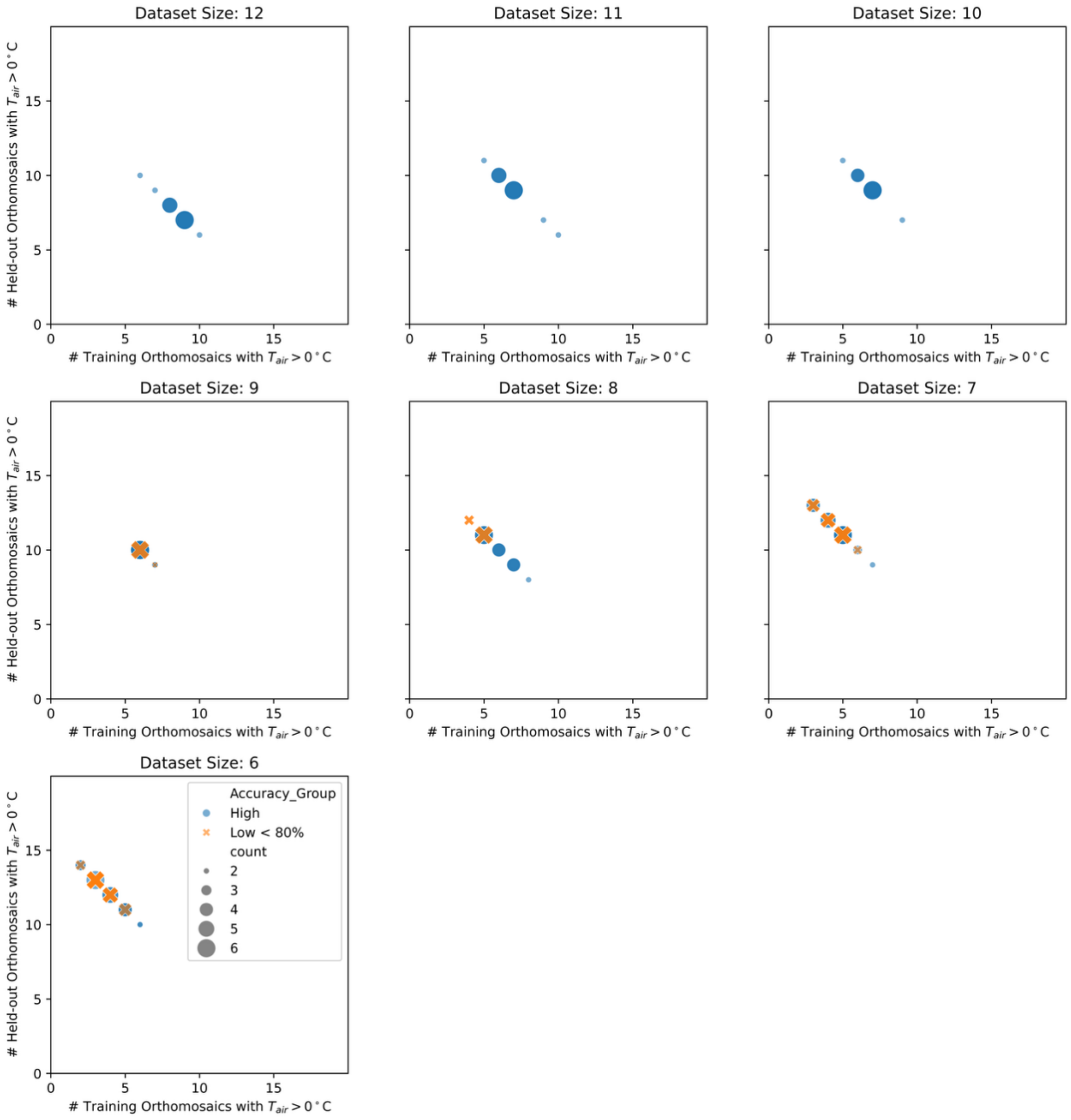

Figure S-9. Number of days with air temperature above freezing within training set VS. Number of days with air temperature above freezing within held-out set for the 20 combinations (10 highest and 10 lowest (<80%) accuracy) for the SVM classifier. Blue dots represent high-accuracy combinations; orange dots represent low-accuracy combinations

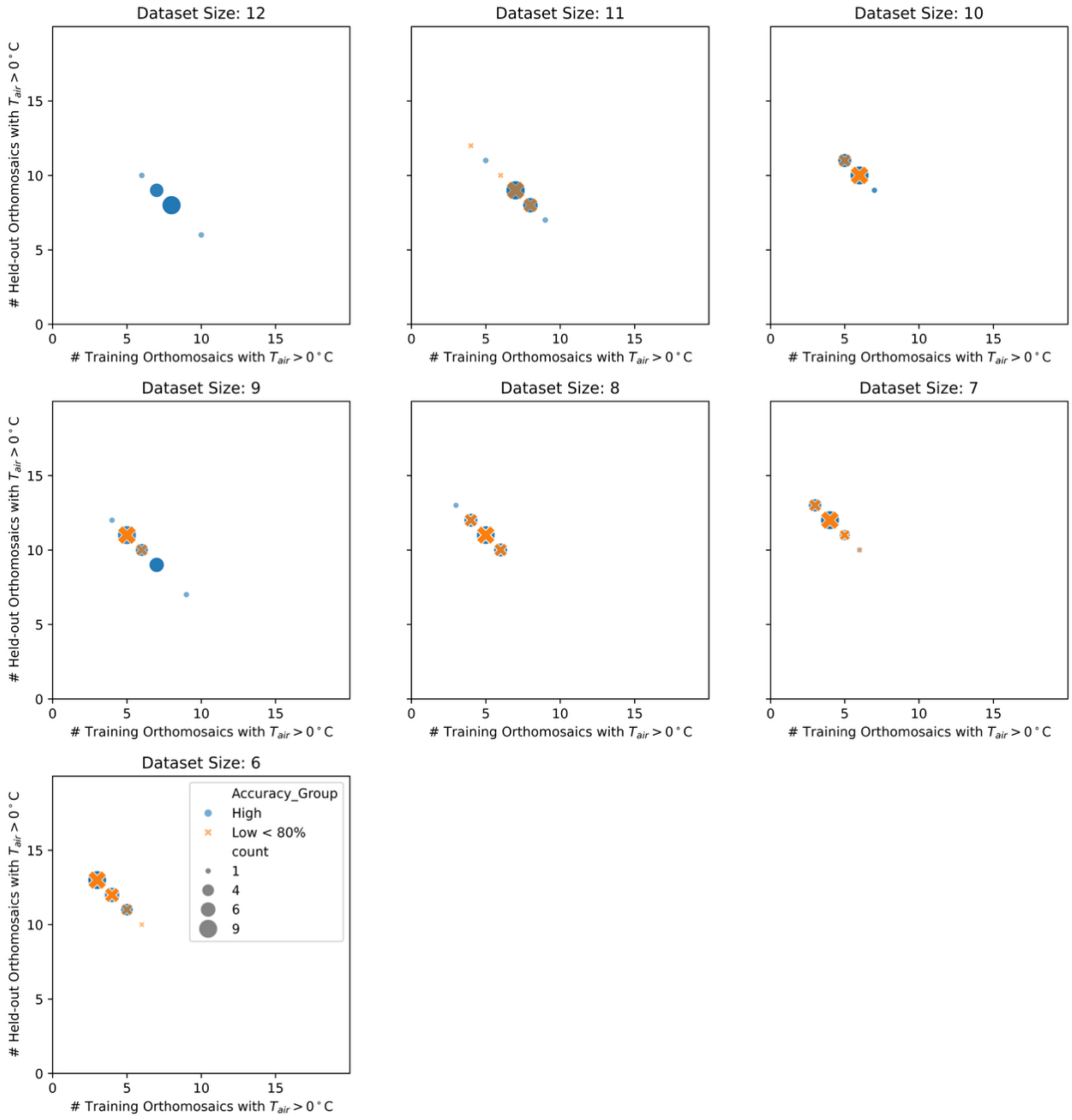

Figure S-10. Number of days with air temperature above freezing within training set VS. Number of days with air temperature above freezing within held-out set for the 20 combinations (10 highest and 10 lowest (<80%) accuracy) for the RF classifier. Blue dots represent high-accuracy combinations; orange dots represent low-accuracy combinations

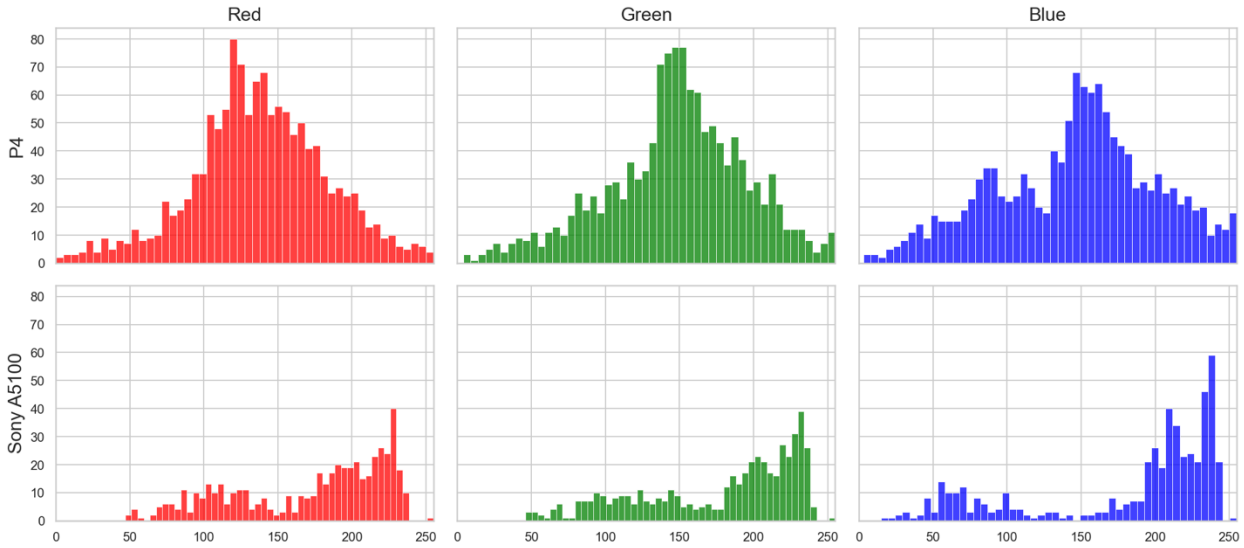

Figure S11. RGB intensity histograms for the P4 and Sony cameras. The y-axis shows the frequency of each value. The x-axis shows intensity ranging from 0 to 255.

Table S3. Confusion matrix for dynamic thresholding approach with minimum threshold of 127

Date	Site	TN	FP	FN	TP
2020_12_23	TF	0	0	15	35
2021_01_25	TF	50	0	0	0
2021_02_20	TF	0	0	2	48
2021_02_23	TF	0	0	2	48
2021_02_24	TF	0	0	6	44
2021_02_26	TF	0	0	4	46
2021_02_28	TF	2	0	1	47
2021_03_01	TF	5	0	3	42
2021_03_03	TF	5	0	8	37
2021_03_07	TF	19	0	7	24
2021_03_10	TF	45	0	3	2
2021_03_11	TF	45	0	3	2
2021_04_02	TF	50	0	0	0
2022_01_12	TF	2	0	0	48
2024_01_18	KF	0	1	0	49
2024_01_23	KF	2	0	0	48
2024_01_27	KF	10	1	1	38
2024_02_06	KF	17	2	5	26
2024_02_08	KF	30	0	6	14
2024_02_12	KF	48	0	1	0

2024_02_26	KF	48	0	0	0
2024_04_05	KF	4	0	2	44
2024_04_08	KF	49	0	1	0
2025_01_27	KF	0	0	8	42

Table S4. Confusion matrix for dynamic thresholding approach with minimum threshold of 90

Date	Site	TN	FP	FN	TP
2020_12_23	TF	0	0	6	44
2021_01_25	TF	50	0	0	0
2021_02_20	TF	0	0	0	50
2021_02_23	TF	0	0	0	50
2021_02_24	TF	0	0	2	48
2021_02_26	TF	0	0	3	47
2021_02_28	TF	2	0	0	48
2021_03_01	TF	5	0	1	44
2021_03_03	TF	4	1	2	43
2021_03_07	TF	16	3	3	28
2021_03_10	TF	45	0	3	2
2021_03_11	TF	45	0	3	2
2021_04_02	TF	50	0	0	0
2022_01_12	TF	0	2	0	48
2024_01_18	KF	0	1	0	49
2024_01_23	KF	2	0	0	48
2024_01_27	KF	7	4	0	39
2024_02_06	KF	17	2	5	26
2024_02_08	KF	30	0	6	14
2024_02_12	KF	48	0	1	0
2024_02_26	KF	48	0	0	0
2024_04_05	KF	3	1	1	45
2024_04_08	KF	49	0	1	0
2025_01_27	KF	0	0	5	45

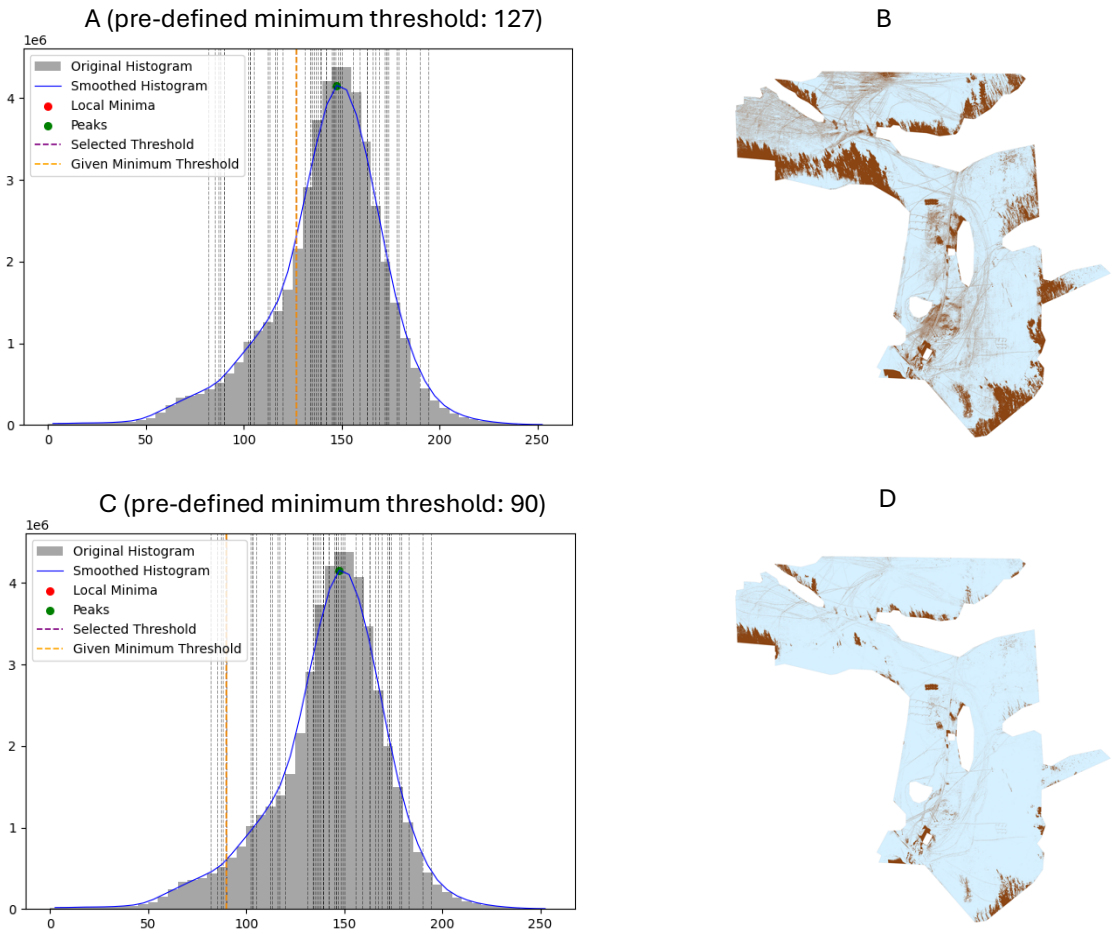

Figure S-12. Histogram of blue band intensity (A, C) and the estimated maps based on the selected threshold (B, D) at Thompson Farm on 2020/12/23. The gray bars represent the original histogram of pixel intensities, and the blue line shows the smoothed version. Local minima and peaks are marked in red and green, respectively. The vertical dashed lines indicate: the selected threshold (magenta), the pre-defined minimum threshold (orange), and the blue band intensity values of randomly sampled pixels (gray dotted lines).

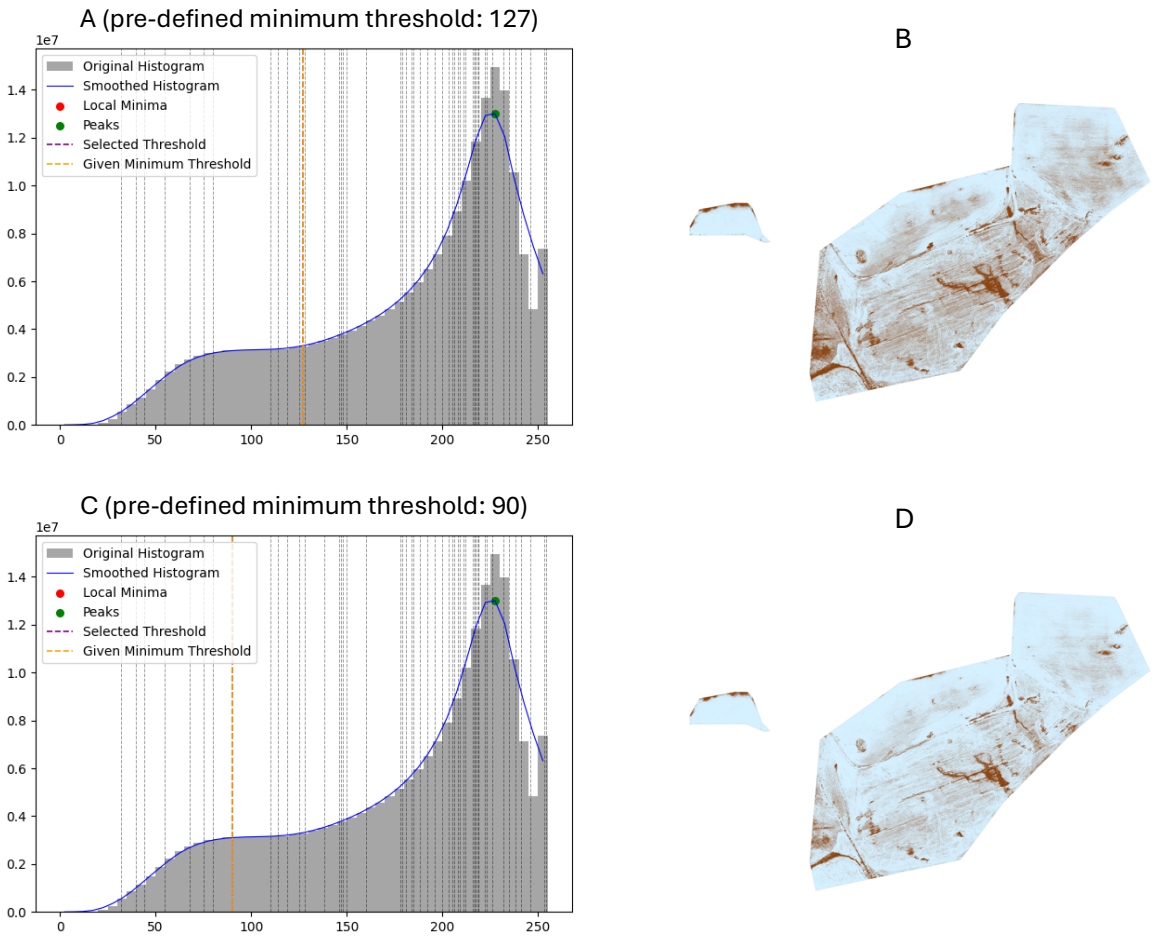

Figure S-13. Histogram of blue band intensity (A, C) and the estimated maps based on the selected threshold (B, D) at Kingman Farm on 2024/01/27. The gray bars represent the original histogram of pixel intensities, and the blue line shows the smoothed version. Local minima and peaks are marked in red and green, respectively. The vertical dashed lines indicate: the selected threshold (magenta), the pre-defined minimum threshold (orange), and the blue band intensity values of randomly sampled pixels (gray dotted lines).

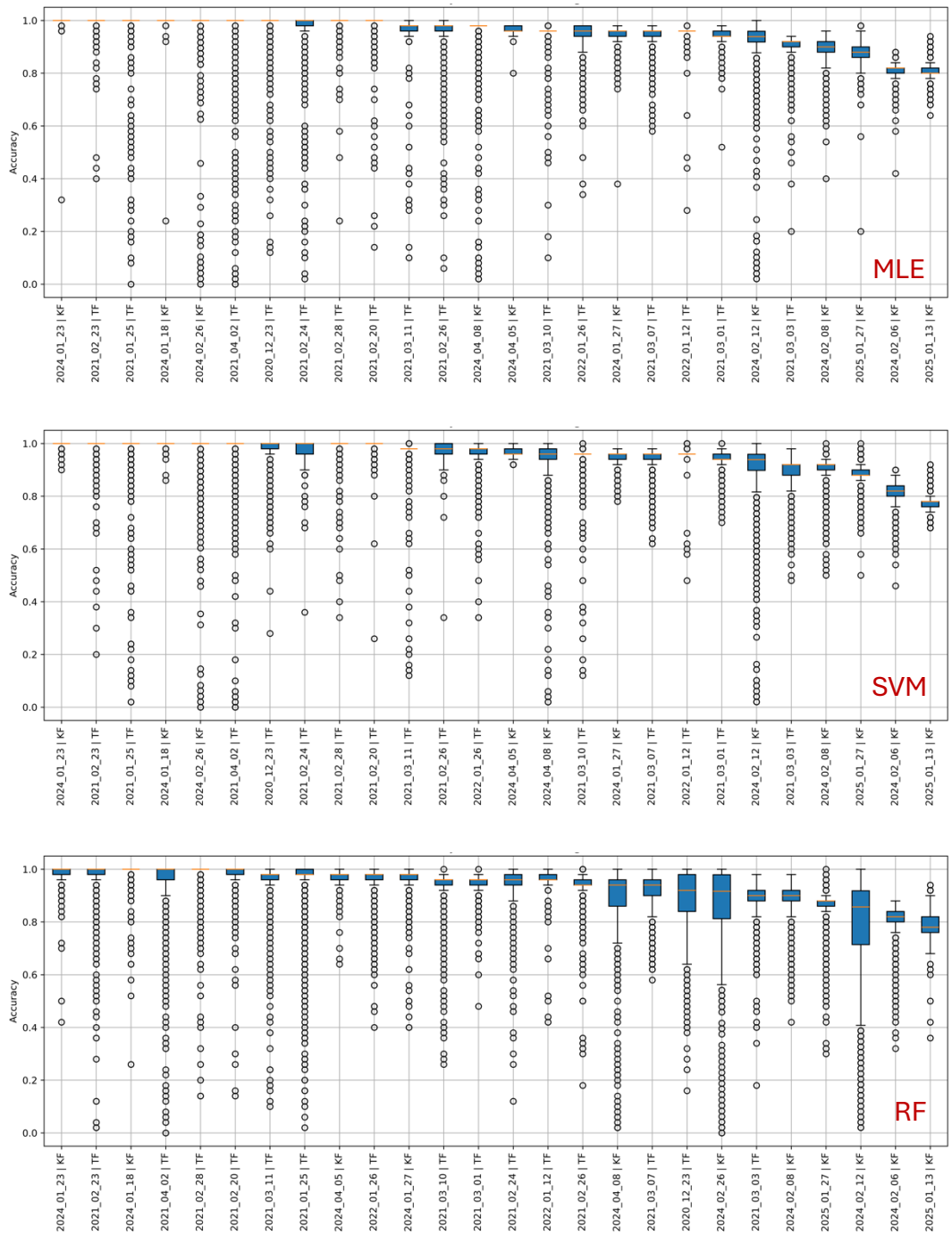

Figure S-14. Accuracy of Experiment 4 models on each orthomosaic across all instances in which that orthomosaic was held-out.

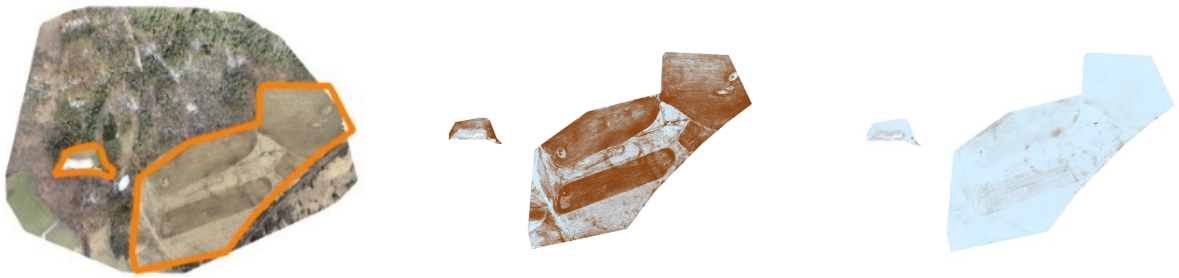

(A) (B)

Figure S-15. Snow cover maps estimated by random forest classifier, trained based on data from 8 orthomosaics, with 60% accuracy (A) and 1% accuracy (B) on 2024/02/26 KF orthomosaic

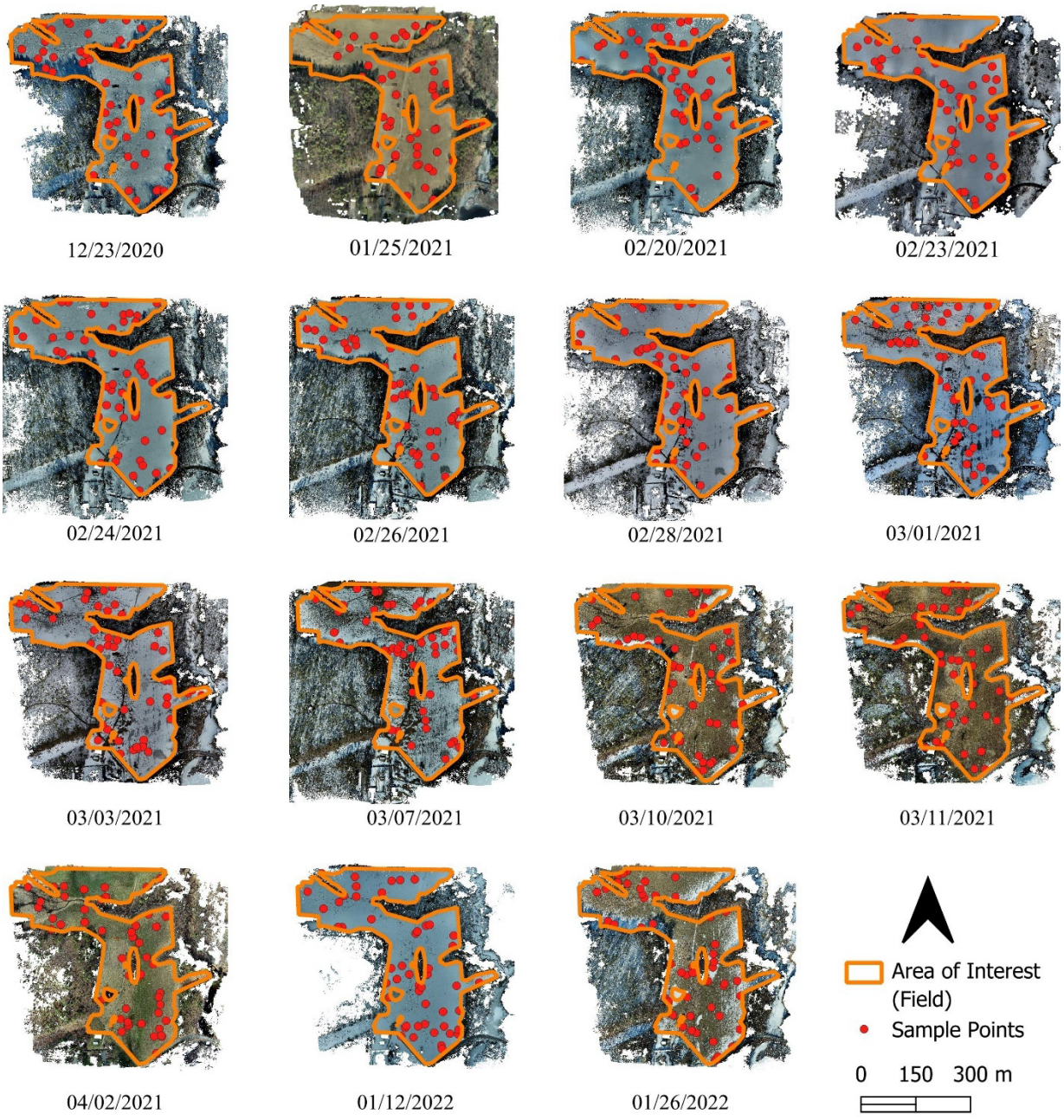

170

Figure S-16. RGB orthomosaics of Thompson Farm acquired with the Phantom 4. Survey dates are shown below each image. Areas of interest are outlined in orange. Random sample points are shown as red dots.

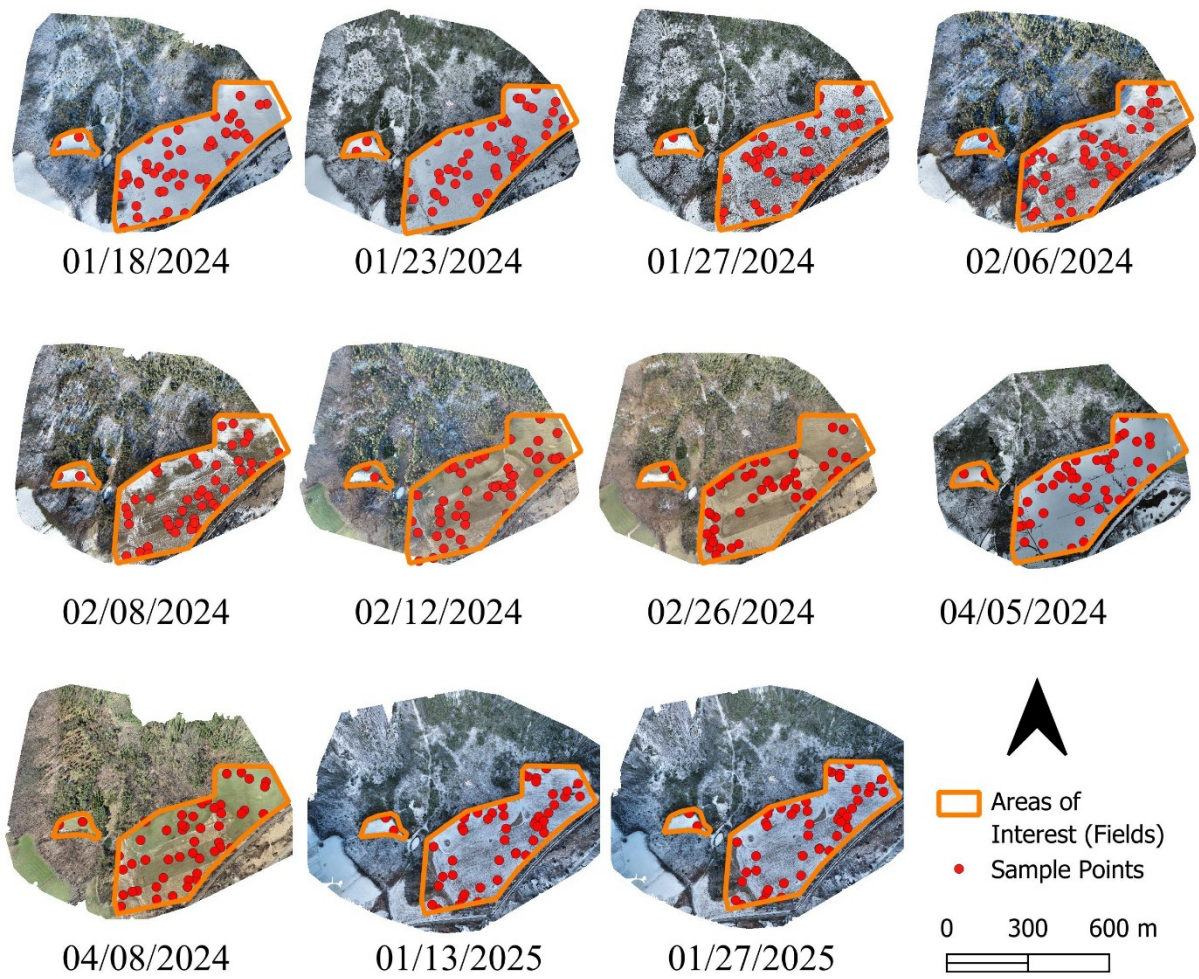

Figure S-17. RGB orthomosaics of Kingman Farm acquired with the Phantom 4. Survey dates are shown below each image. Areas of interest are outlined in orange. Random sample points are shown as red dots.

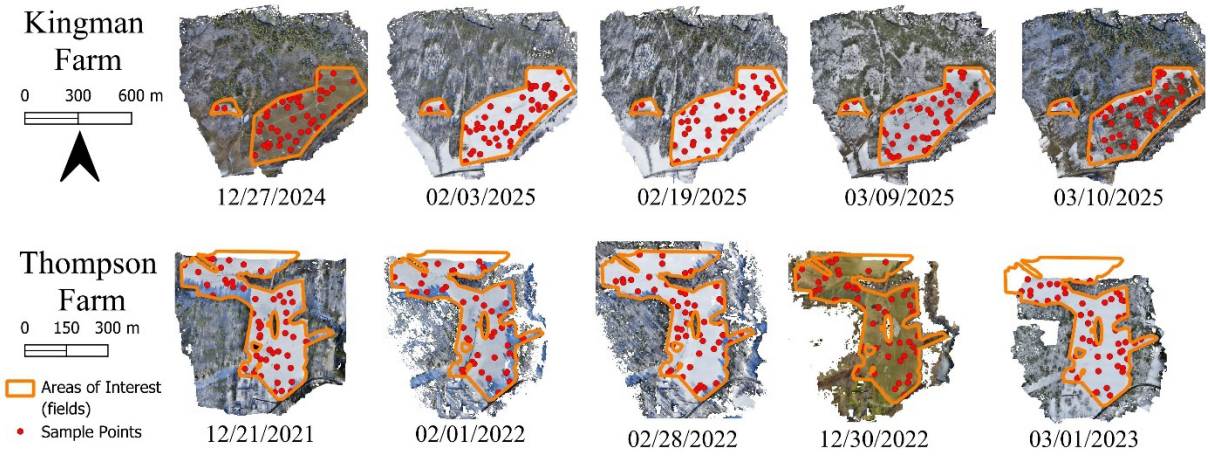

Figure S-18. RGB orthomosaics of Kingman Farm (top row) and Thompson Farm (bottom row) acquired with the Sony A5100 camera. Survey dates are shown below each image. Areas of interest are outlined in orange. Random sample points are shown as red dots

185